Simulation of thermal-field directed self-assembly of epitaxial quantum dots

Chandan Kumar[a] and Lawrence H. Friedman
Department of Engineering Science and Mechanics, Pennsylvania State University, 212 Earth and Engineering Sciences Building, University Park, Pennsylvania 16802

(Received 19 September 2006; accepted 2 March 2007; published online 4 May 2007)

Thermal-field directed self-assembly (TDSA) of epitaxial self-assembled quantum dots (SAQDs) is the method of using spatially varying temperature patterns to influence SAQD growth kinetics and ultimately the order and positions of SAQDs. The effectiveness of TDSA in enhancing the size and spatial order or precision placement of single dot or dot cluster is investigated via a two dimensional (one dimensional surface) finite element based model of Ge dots grown on Si. Three different cases of heating are studied, namely, spatially constant heating, spatially periodic heating, and a Gaussian shaped hot spot. Statistical measures are used to study the evolution of quantum dot heights and spacings between the quantum dots for different temperatures and heating cases. Spatially periodic heating is investigated for a wavelength of about 185 nm corresponding to the wavelength of an excimer laser. In order to investigate the effectiveness of spatially periodic heating in enhancing the spatial and size order of the SAQD array, the results are compared with those obtained from spatially uniform heating. Simulations using Gaussian shaped hot spot are performed to demonstrate its effectiveness in placing a distinct dot at a desired location. Results from the simulations indicate that spatially periodic heating proves to be an effective means for producing an array of uniformly sized and spaced quantum dots for a broad range of temperatures. Also, the results from the simulations using Gaussian shaped hot spots show that such a form of heating can effectively place a distinct quantum dot near a desired location for a broad range of temperature values. © *2007 American Institute of Physics*. [DOI: 10.1063/1.2723871]

I. INTRODUCTION

Growth of self-assembled semiconductor quantum dots is of particular interest in the development of quantum dot based devices such as quantum computing architectures, laser diodes, and other optoelectronic devices.[1–6] In Ref. 7 it was demonstrated that it may be possible to use spatially varying surface temperatures to influence the formation of self-assembled quantum dots (SAQDs), leading to enhanced spatial and size order, a process dubbed *thermal-field directed self-assembly*. Here, this process is investigated further using a finite element based simulation to elucidate the method and to motivate and guide experiments. Simulations are carried out for Ge dots grown on Si, a system that is often used as a model system but also of great technological interest.

The formation of SAQDs is initiated by the lattice mismatch in the heteroepitaxial systems such as Ge_xSi_{1-x} on Si and $In_xGa_{1-x}As$ on GaAs. The ordering and precision placement of these SAQDs have been matters of concern in fostering the development of the quantum dot based devices.[8] There are two types of order, spatial and size. Spatial order is concerned with the uniformity of the spacings between the SAQDs and size order is concerned with the uniformity in the size of the SAQDs. In this respect, one would like to either generate large arrays of regularly spaced and/or regularly sized SAQDs or be able to place SAQDs in desired locations. Controlling self-assembly in such a fashion to produce this outcome is known as "directed self-assembly."

A few previous examples of directed-self assembly of quantum dots are the preferential nucleation of SAQDs above intersection points of an array of misfit dislocations,[9] nucleation of quantum dots on etched mesas,[10] the ability to nucleate SAQD clusters using a focused ion beam (FIB),[11] and the ability to grow Ge islands at desired locations by creating carbon based templates on a Si substrate.[12]

In Ref. 7 numerical simulations suggested that a spatially periodic temperature profile can produce an array with greatly enhanced spatial and size orders and that localized heating can produce a distinct quantum dot. This form of directed self-assembly is based on SAQD formation kinetics and works by modulating the local diffusivity of surface atoms. At present, there is no experimental confirmation of thermal-field directed self-assembly. To motivate and guide experiments and to further assess the effectiveness of thermal-field directed self-assembly, the results of further simulations with quantitative analysis are presented here.

Three cases of heating are simulated: (1) spatially uniform heating, (2) spatially periodic heating, and (3) spatially localized heating. Spatially uniform heating simulations are used as the control. Spatially periodic heating is assessed for its ability to enhance spatial and size orders of a quantum dot array. Finally, localized heating is assessed for its ability to create a distinct, precisely placed dot. These three cases are looked at for annealing times ranging from 0 to 200 s, and for temperatures ranging from 350 to 550 °C.

[a]Electronic mail: cuk137@psu.edu

It is found that spatially varying heating leads to bimodal populations of self-assembled quantum dots. "Large" dots form near the site of maximum temperature and "small" dots form away from the sites of maximum temperature. For the spatially periodic heating case, the small dot population vanishes after sufficient annealing time. For all other instances, it is hypothesized that the small dots will not degrade device performance provided that they are sufficiently distinct in size, as dot size is a crucial parameter for determining quantum dot excitation energies and capacitances. Thus, in addition to assessing the order of the large dots, it is also necessary to determine how distinct in size they are from the small dots.

The rest of this article is organized as follows. Model details are given in Sec. II. Simulation results for the three cases of heating are presented in Sec. III. Analysis of the resulting SAQD order is presented in Sec. IV. Section V presents the conclusions.

II. MODEL

The model description has two parts: physical and numerical. First, the physical/mathematical model is discussed. Then the numerical implementation using COMSOL MULTIPHYSICS (Ref. 13) is discussed.

A. Physical/mathematical model

The physical model is the same as in Ref. 7, and it is similar to the one in Ref. 14. The formation of SAQDs is modeled as resulting from unstable film growth. The unstable growth results from a mismatch strain ϵ_0 with respect to the substrate and the surface. Evolution of the film height, $h(x,t)$, takes place due to surface diffusion that is driven by a diffusion potential μ. The model is implemented in two dimensions in the x-y plane, with one dimensional (1D) evolving surface. The normal component of the velocity of the growing film depends on both the diffusion potential gradient and the flux of new material onto the surface.

$$v_n = n_y \frac{\partial h}{\partial t} = \nabla_s \cdot D \nabla_s \mu + n_y Q, \tag{1}$$

where n_y is the y component of the surface normal $\hat{n}$, ∇_s is the surface gradient, $\nabla_s \cdot$ is the surface divergence, D is the surface diffusion coefficient, and Q is the flux of new material onto the surface. The surface diffusion coefficient is given by

$$D = \frac{D_s C_s}{k_B T} \exp\left[-\frac{\Delta E}{k_B T} \right], \tag{2}$$

where D_s is the intrinsic surface diffusivity, C_s is the mobile surface atoms per unit area, k_B is the Boltzmann's constant, T is the absolute temperature, and ΔE is the surface diffusion activation energy. The effect of spatially varying temperature enters through Eq. (2). Ideally, the surface velocity [Eq. (1)] should be modified to include a noise term; however, such a term complicates simulation and makes implementation in COMSOL MULTIPHYSICS difficult. Thus, noise is incorporated into the initial conditions only.

The diffusion potential μ is given by

$$\mu = \Omega \left[\omega - \kappa(\gamma + W) + n_y \frac{dW}{dy} \right], \tag{3}$$

where Ω is the atomic volume, ω is the strain energy density at the free surface, κ is the total surface curvature, γ is the surface energy density, and W is the wetting potential that is a function of the film height h and ensures wetting of the substrate.[15] The thickness dependent model for wetting potential is taken from Ref. 14 and is given by $W(h)=B/h$, where B is a material constant and h the film height.

Linear isotropic elasticity is used to calculate the local strain energy density, ω. The strain is composed of an initial eigenstrain $\{\epsilon_0\}$ plus a displacement strain, $\{\epsilon_d\}$, $\{\epsilon\}=\{\epsilon_0\}+\{\epsilon_d\}$, where $\{\epsilon\}=\lfloor \epsilon_x\ \epsilon_y\ \epsilon_z\ \gamma_{xy}\ \gamma_{xz}\ \gamma_{yz} \rfloor^T$. The eigenstrain, $\{\epsilon_0\}=\lfloor \epsilon_0\ \epsilon_0\ \epsilon_0\ 0\ 0\ 0 \rfloor^T$, is due to the lattice mismatch between the film and substrate, and it is present in the reference displacement field configuration, $\mathbf{u}=\mathbf{0}$. The displacement strain is defined in the usual way for linear elasticity, $(\epsilon_d)_i = \partial u_i/\partial x_i$, and $(\gamma_d)_{ij} = \partial u_i/\partial x_j + \partial u_j/\partial x_i$, where $\mathbf{u}$ is the displacement.

The stress state in the film is related to the strain state by Hooke's law for an isotropic material. Linear isotropic plane-strain elasticity is used because it will give the appropriate linear behavior when ripple-patterned growth instabilities first set in.[16] Hence, the stress state existing in the film can be rewritten as $\{\sigma\}=[E]\{\epsilon\}$. The nonzero strain components for plane-strain displacement plus volumetric eigenstrain are $\epsilon_x = (\epsilon_d)_x + \epsilon_0$, $\epsilon_y = (\epsilon_d)_y + \epsilon_0$, $\epsilon_z = \epsilon_0$, and $\gamma_{xy} = (\gamma_d)_{xy}$. The nonzero stress components are normal stresses, $\sigma_i = \Sigma_{j=x,y,z}(\lambda + 2\mu\delta_{ij})\epsilon_j$ $(i=x,y,z)$ and shear stress, $\tau_{xy} = \mu(\gamma_d)_{xy}$, where λ is Lamé's constant and μ the shear modulus. Elastic equilibrium is calculated using the plane-strain equilibrium equations, $\partial_x \sigma_x + \partial_y \tau_{xy} = 0$, and $\partial_x \tau_{xy} + \partial_y \sigma_y = 0$ along with periodic boundary conditions in the x direction, and traction-free boundary condition on the free surface. The actual strain energy density is $1/2\{\sigma\}^T\{\epsilon\}$. However, an offset $\omega_0 = 1/2(9\lambda + 6\mu)\epsilon_0^2$ is subtracted from the actual strain energy to give

$$\omega = \tfrac{1}{2}\{\sigma\}^T\{\epsilon\} - \omega_0. \tag{4}$$

This makes $\omega=0$ when $\mathbf{u}=\mathbf{0}$. The offset does not effect the film growth because only the gradient of ω is relevant [see Eqs. (1) and (3)].

Periodic boundary conditions are implemented to mitigate the effects of the simulation's finite size. The heating source has not been specifically modeled. It is assumed that one can create a spatially varying temperature profile and a characteristic wavelength as small as $\lambda^* = 185$ nm, a wavelength achievable using an excimer laser. The periodic temperature profile is thus

$$T(x) = T_{\text{base}} + \Delta T \cos^2(\pi x/\lambda^*), \tag{5}$$

where λ^* is the heating wavelength. The local heating profile is approximately Gaussian,

$$T = T_{\text{base}} + \Delta T \exp[-\sin^2(kx)/(2k^2\Delta x^2)], \tag{6}$$

where $k=\pi/w$, w is the simulation width, and Δx characterizes the width of the hot spot.

Random initial conditions are used to "seed" SAQD growth. Initially, the surface is nominally flat with a random atomic-scale fluctuation,

$$h(x,0) = h_0 + \chi(x). \tag{7}$$

The random part $\chi(x)$ is generated by smoothing of a discrete grid of $2N+1$ random points $\{X_i\}$ that are taken from uniform distribution over the interval $[-1/2, 1/2]$.

$$\chi(x) = \chi_0 \sum_{n=1}^{N} A_n \cos(2\pi nx/w) + B_n \sin(2\pi nx/w), \tag{8}$$

$$A_n + iB_n = \frac{1}{2N+1} \sum_{m=1}^{2N+1} e^{-2\pi in(m-1)/(2N+1)} X_m, \tag{9}$$

and w is the width of the simulation. The resulting noise function $\chi(x)$ thus gives a function that fluctuates to $\pm\chi_0/2$ with a spatial correlation length of about w/N.

B. Numerical implementation

Equations (1) and (3) and elastic equilibrium combine to form a differential algebraic system. Numerical simulations were performed using COMSOL MULTIPHYSICS,[13] although the model was developed in a previous version known as FEMLAB. At the time the model was developed and implemented, FEMLAB did not directly support moving boundaries, so the elasticity part of the problem is solved using a time dependent coordinate transformation. This is done by a linear mapping of the x-y space into the dimensionless rectangular ξ-η space. In the real space the substrate/film have a width w_i and a height h_i ($i=s$ for substrate or f for film). In calculation space, the substrate/film mesh has a width $l_{x,i}$ and height $l_{y,i}$. Thus within the film or substrate, $x = w/l_x(\xi - \xi_0) + x_0$, and $y = h(\xi)/l_y(\eta - \eta_0) + y_0$. This transformation solves the moving boundary problem but it requires a great deal of equation manipulation to implement. Implementation in COMSOL MULTIPHYSICS (Ref. 13) is also helped by expressing the governing equations in the form of flux conservation equations,

$$\nabla \cdot \Gamma = F, \tag{10}$$

for algebraic equations with no explicit time dependence such as elasticity and diffusion potential, or

$$d\frac{\partial}{\partial t}u + \nabla \cdot \Gamma = F, \tag{11}$$

for the time dependent equation such as surface diffusion. This procedure is complicated by the coordinate transformation.

III. RESULTS

The model described in Sec. II is used to carry out several simulations of the film height evolution process for the three different cases of heating. Each simulation is characterized by a base temperature (T_{base}) and a temperature maximum (T_{max}) or the corresponding temperature amplitude $\Delta T = T_{max} - T_{base}$ [as in Eqs. (5) and (6)]. For the control simulations (uniform temperature) $T = T_{max} = T_{base} + \Delta T$. In Ref. 7, simulations were done for $\Delta T = 200\ ^\circ$C and a single random initial noise pattern was used. In this work, simulations have been carried out for various additional ΔT values and random initial noise patterns in order to statistically characterize the film height evolution process in thermal-field directed self-assembly (TDSA). The effect of ΔT and annealing time (t) is analyzed on the self-assembly process. The simulation parameters and a few representative simulations of the three aforementioned cases of heating are discussed in the following paragraphs.

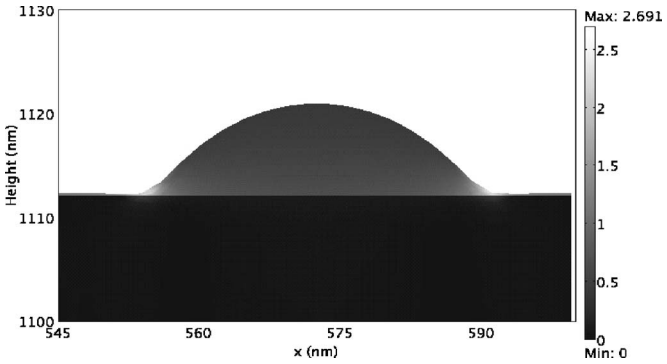

FIG. 1. Close up of a single dot formed after time $t=100$ s as a result of spatially uniform heating with $T=350\ ^\circ\text{C}+200\ ^\circ\text{C}$ (noise 1). Gray scale indicates the ratio between the actual strain energy density $1/2\{\sigma\}^T\{\epsilon\}$ and ω_0 [see Eq. (4)].

The three mentioned cases are simulated for a range of temperatures for Ge dots on Si substrate. For each of the three cases, simulations are carried out for $T_{base}=350\ ^\circ$C and $\Delta T=25$, 50, 100, 125, 138, 150, 175, and 200 °C. Each simulation is carried out on a periodic simulation cell width $w=1.112\ \mu$m and a substrate height of $h_s=1.112\ \mu$m. For the periodic temperature profiles, $\lambda^* = w/6 = 185.3$ nm in Eq. (5). For the localized heating, $\Delta x = 111.2$ nm in Eq. (6). The initial film height is always $h_0=2.75$ ML (monolayer) $=7.47$ Å. Then Ge is deposited at a rate of 0.25 ML for the first 2 s. The initial nominally flat film has an additive noise given by Eq. (8) with $\chi_0=1$ Å and $N=200$ for noise 1 and $N=100$ for all other initial noise patterns. The film surface evolution is simulated for a duration $t=222$ s.

Other simulation parameters are as follows. As given in Ref. 16, the Young moduli are $E_{Ge}=1.362\times10^{12}$ and $E_{Si}=1.660\times10^{12}$ dyn/cm^2, the Poisson ratios are $\nu_{Ge}=0.198$ and $\nu_{Si}=0.217$, the mismatch strain is $\epsilon_0=-0.0418$, the atomic volume is $\Omega=2.27\times10^{-23}$ cm^3, the surface energy density is $\gamma=1927$ ergs/cm^2, the intrinsic diffusivity is $D_s=8.45\times10^{-6}$ cm^2/s, the surface concentration is $c_s=1.25\times10^{15}$ cm^{-2}, and the activation energy is $\Delta E=1.33\times10^{-12}$ erg. The wetting potential is given by $W(h)=(7.59\times10^{-7}$ erg/cm$^2)/h$. The initial height fluctuation is $\chi_0=1$ Å.

The various simulations indicate that higher ΔT values give more pronounced ordering. Hence, a few simulation results for $\Delta T=200\ ^\circ$C are discussed in the following lines. These simulations were initially reported in Ref. 7 and a few results are shown in Figs. 1–4, with emphasis on various statistical tools that are to be used for analysis in the following section. In these simulations, noise 1 with $N=200$ has been used for the random initial height fluctuations. Figure 1 shows the close up of a single dot with the ratio of the actual

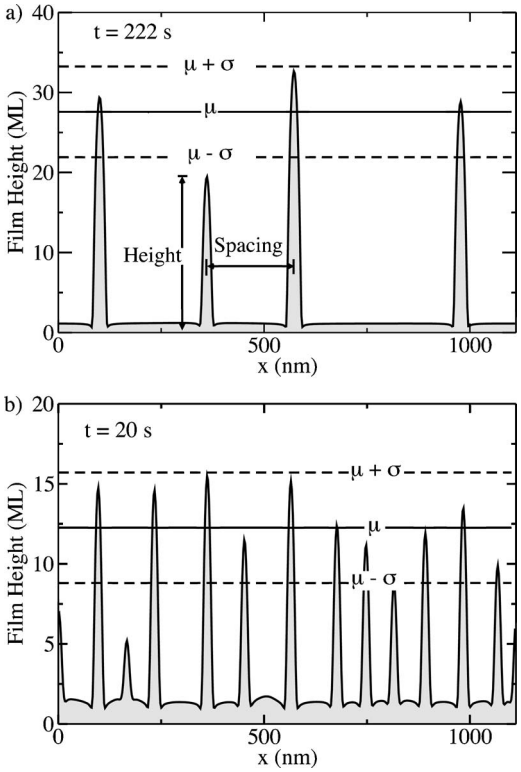

FIG. 2. Simulation results for uniform heating with $T=350\ ^{\circ}\mathrm{C}+200\ ^{\circ}\mathrm{C}$ (noise 1). Dashed lines indicate quantum dot heights, one standard deviation away above and below the mean height. The mean height is indicated by a solid line.

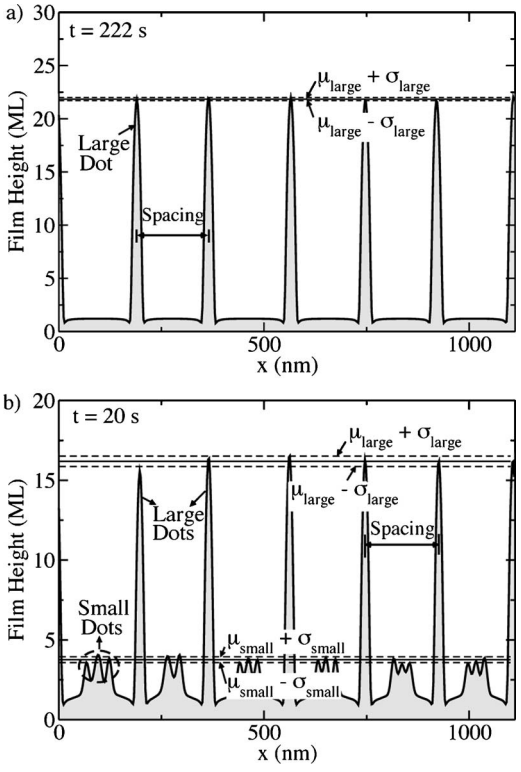

FIG. 3. Simulation results for spatially periodic heating with $\Delta T=200\ ^{\circ}\mathrm{C}$, $T_{\mathrm{base}}=350\ ^{\circ}\mathrm{C}$ (noise 1) for (a) $t=222$ s and (b) $t=20$ s. Dashed lines indicate the quantum dot heights one standard deviation above and below the mean height. In (b), there is a bimodal population of "small" and "large"quantum dots.

strain energy density $1/2\{\sigma\}^{T}\{\epsilon\}$ to ω_0 plotted for time $t=100$ s and spatially uniform heating with temperature $T=T_{\mathrm{base}}+200\ ^{\circ}\mathrm{C}$. In contrast to the relaxed state in the region near the peak of the quantum dot, the regions near the two valleys show higher values of strain energy density due to higher stress concentration in these regions.[16] Figures 2–4 are not to scale as the dot aspect ratios are stretched in the vertical direction for clarity. Figure 2 shows results from a uniform temperature simulation with $T=T_{\mathrm{base}}+\Delta T=550\ ^{\circ}\mathrm{C}$. The growth process results in an array of quantum dots with varying sizes and interquantum dot spacings. In Fig. 3, film height evolution is shown at two instants of time for the case of spatially periodic heating with temperature difference $\Delta T=200\ ^{\circ}\mathrm{C}$. The simulation clearly shows enhancement in size and spatial orders of the quantum dots after some ripening. The periodic heating simulations are characterized by the occurrence of large and small dots for smaller annealing times. For the current case, $t=20$ s is one such instant where both large and small dots coexist. However, the small dots disappear for larger annealing times. Here, $t=222$ s is one such instant where small dots have completely disappeared. Figure 4 shows the film growth in the presence of a Gaussian shaped hot spot of width 222 nm and temperature difference $\Delta T=200\ ^{\circ}\mathrm{C}$. A distinct central dot is formed around a desired location and is surrounded by a small dot cluster.

The different statistical measures such as mean height of the quantum dots (μ), spacing between two consecutive quantum dots and dot height standard deviation (σ) as shown in Figs. 2 and 3 with reference to small and large dots, and

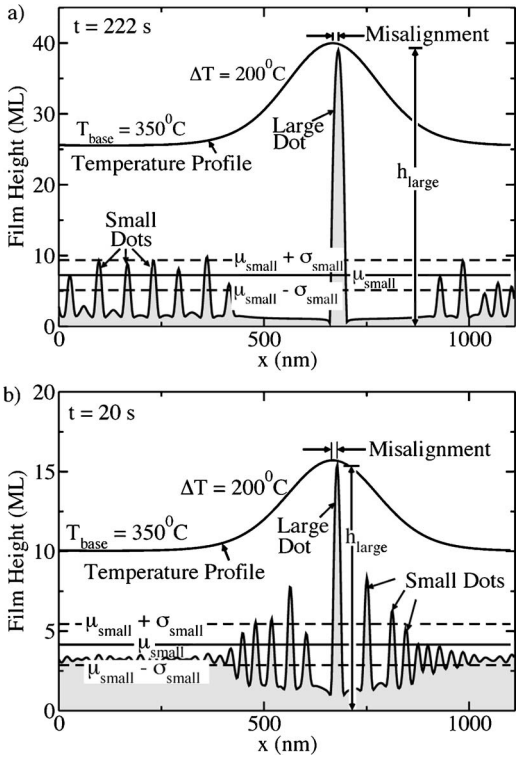

FIG. 4. Simulation results for Gaussian shaped localized heating with $\Delta T=200\ ^{\circ}\mathrm{C}$, $T_{\mathrm{base}}=350\ ^{\circ}\mathrm{C}$ (noise 1). Dashed lines indicate the height of the small quantum dots, one standard deviation above and below their mean height. Mean height is indicated by a solid line.

misalignment as shown in Fig. 4 have been used for the purpose of analysis and will be explained in the following section.

IV. QUANTITATIVE ANALYSIS OF TDSA

In Ref. 7, it was demonstrated that TDSA can lead to fairly well ordered SAQD arrays in the case of a periodic temperature profile and to reasonably accurate placement of a single dot in the case of a Gaussian temperature profile. However, it is also useful to assess the effectiveness of the periodic and Gaussian temperature profiles quantitatively and as a function of the temperature variations ΔT and the annealing times t. First, the periodic temperature profile is investigated for its effectiveness in producing size and spatial order enhancements. Then, the Gaussian profile is investigated for its ability to produce a well-placed distinct quantum dot. The following analysis takes into account different initial random height fluctuations.

A. Effectiveness of periodic heating

The effectiveness of a periodic temperature profile to produce enhanced size and spatial orders of SAQDs is assessed using a uniform temperature profile with the same T_{max} as a control. While the control uniform temperature profile leads to an array of dots of varying sizes (Fig. 2), the periodic temperature profile leads to a bimodal distribution of large ordered dots and small disordered dots [Fig. 3(b)]. The large dots are formed essentially near the regions where ΔT is maximum and the small dots are formed at sites away from the ones where ΔT is maximum. In the following analysis, the large dots are treated as desirable, while the small dots are assessed for their potential to interfere with the performance of the large dots. Thus, the quality of the large dots is assessed for uniformity of height, dot spacings, and distinctness from the background small disordered dots. It is assumed that the small background dots will only interfere with the performance of the large ordered dots if there is significant overlap in their size distribution as their size determines their interesting electronic properties, namely, energy level quantization and capacitance. The SAQD order is found to be a function of both the height of the temperature profile characterized by ΔT and the annealing time t, and both size and spatial orders are investigated.

In the following analysis, it is necessary to track the evolution of the large dots and small dots separately. The large dots are identified using a film height profile corresponding to a large t value. Once identified, these dots can be tracked for all t values, and separate statistical measures are reported for the large and remaining small dots.

1. Size order

Size order is measured by finding the means and standard deviations of the dot heights. It is worth noting that one obtains similar results by studying the dot widths. Figure 5 shows the trends in dot heights as a function of annealing time for three ΔT values. The mean height values and the

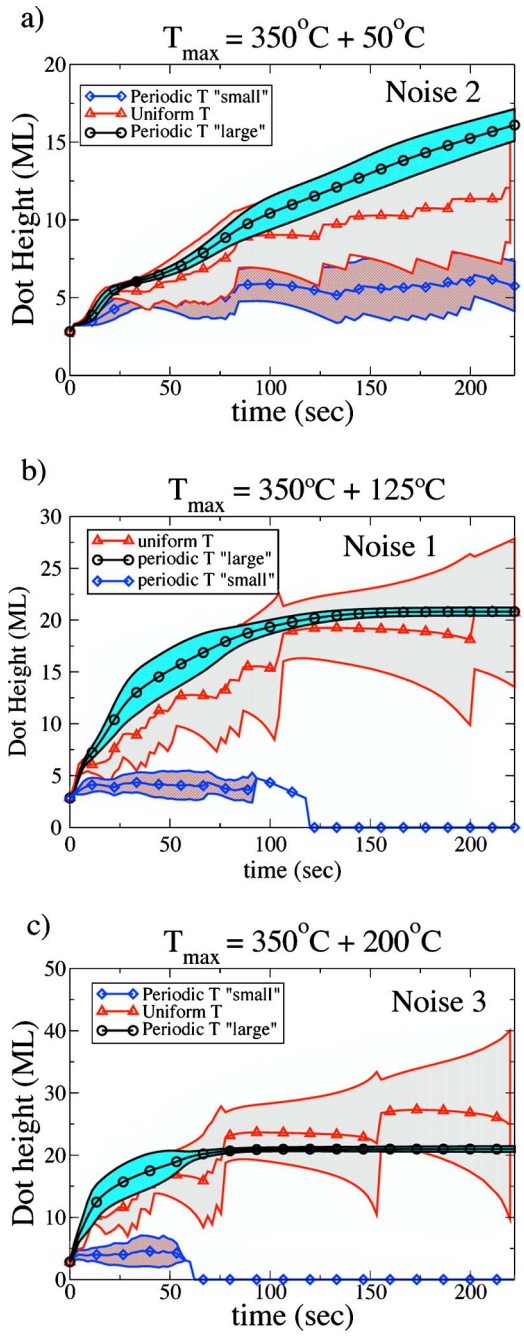

FIG. 5. (Color online) Statistical characterization of the quantum dot heights. (a) ΔT=50 °C. (b) ΔT=125 °C. (c) ΔT=200 °C. Symboled lines indicate mean heights. Shading indicates one standard deviation above and below the mean height. Values are shown for "large" and "small" dots [see Fig. 3(b)] and for uniform temperature results (see Fig. 2).

standard deviations are plotted for large dots and small dots that result from periodic heating along with the values for the control uniform temperature case.

For the control case (uniform temperature), the dot height mean and standard deviations increase with time as ripening proceeds. For the spatially periodic heating case, the large dot height mean and standard deviations grow initially, but after sufficient time, a relatively constant value with a tight distribution is achieved. The small dots exhibit a little growth of their mean height and standard deviations but eventually vanish as their material is siphoned off to the larger dots.

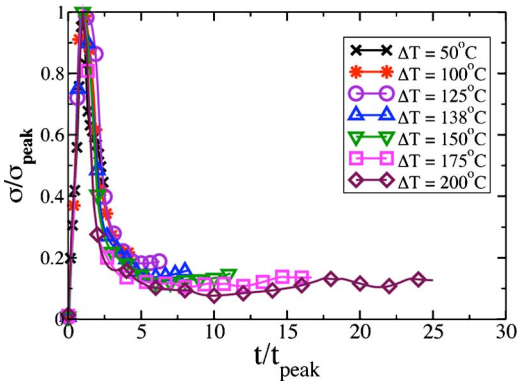

FIG. 6. (Color online) Standard deviation of the "large" quantum dot heights for spatially periodic heating (noise 1). Plots are scaled by σ_{peak} and t_{peak}.

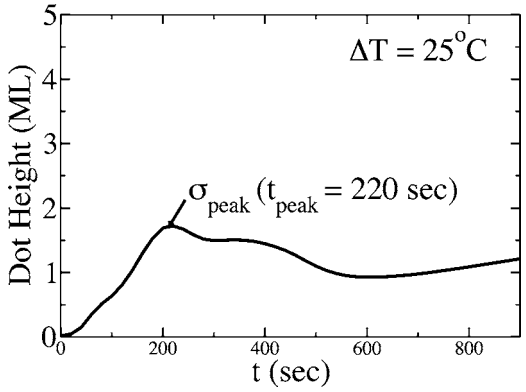

FIG. 8. Standard deviation of "large" quantum dot heights for spatially periodic heating with ΔT=25 °C (noise 1).

Further analysis for different ΔT values demonstrates the following. For all shown ΔT values, significant size order improvement is demonstrated as the dot height standard deviation is smaller compared with the control (uniform temperature) case. In general, larger temperature differences (ΔT) and larger annealing times (t) lead to better dot height order. Finally, the large dots are very distinct from the small dots for most ΔT values and annealing times.

Dot height standard deviations as a function of time are shown in Fig. 6 for ΔT ranging from 50 to 200 °C. Shown results correspond to noise 1, but other initial height fluctuations produce the same behavior. For all ΔT's, the time dependence of the standard deviation is the same; first, there is an initial increase in dot height standard deviation, followed by a decrease. In Fig. 6, the curves are scaled so that all peaks coincide. Each curve can be characterized by the peak standard deviation, σ_{peak}, and the final standard deviation, i.e., σ_{end} at t=222 s. These measures that characterize the overall behavior are shown in Fig. 7. The trends in σ_{peak} and σ_{end} are shown for the three different noise realizations. The trend in σ_{peak} follows no obvious pattern. However, the trend in σ_{end} is to monotonically decrease with ΔT. While it is difficult to explain the trend in σ_{peak}, the trend in σ_{end} is intuitive as greater ΔT gives more pronounced thermally directed self-assembly. For noise 3, the σ_{peak} and σ_{end} values at ΔT=50 °C coincide because the standard deviation curve did not reach its maximum value within the considered annealing time range. It is worthwhile to note that a small σ_{peak} is seen for temperatures as low as 25 °C (Fig. 8). Thus indicating that even at lower temperatures an improvement in the size order occurs at later stages of evolution.

Finally, in Fig. 9, it is demonstrated that for most annealing times and ΔT values, the large dots are distinct from the small dots. The distinctness of the dot populations was inspected visually from the simulation results. However, it is useful to have a single quantitative measure. The following measure of distinctness is suitable:

$$d = \frac{(\mu_{large} - \sigma_{large}) - (\mu_{small} + \sigma_{small})}{\mu_{large} + \sigma_{large}}, \tag{12}$$

where d denotes distinctness, μ_{large} and σ_{large} are the mean and standard deviations of the heights of the large dots, respectively, and μ_{small} and σ_{small} are the mean and standard deviations of the heights of the small dots, respectively. In Fig. 3, $\mu_{large} \pm \sigma_{large}$ and $\mu_{small} \pm \sigma_{small}$ have been shown for ΔT=200 °C at two different stages of time. Although what distinctness value is acceptable would depend upon applications, here, an arbitrary value of 0.5 is defined. This cutoff also agrees with visual inspections of the simulation results. A typical case with distinctness of 0.5 is shown in Fig. 10. Any value of distinctness greater than 0.5 can be considered as a "usable distinctness" value since it reflects sufficient separation between the large and the small quantum dot

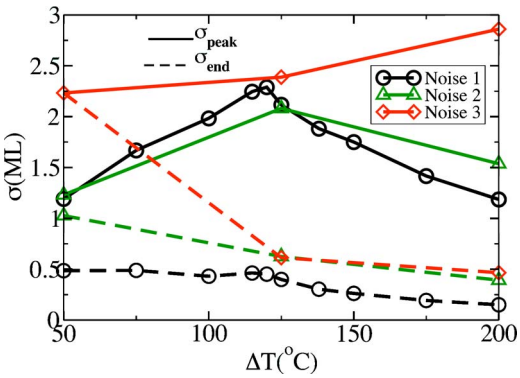

FIG. 7. (Color online) "Large" quantum dot height standard deviations for spatially periodic heating for three realizations of random initial conditions. Both peak and end values (see Fig. 6) shown vs time.

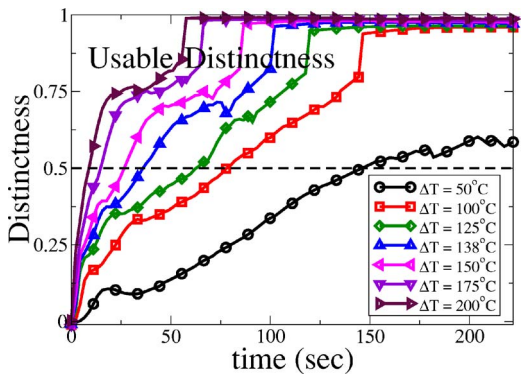

FIG. 9. (Color online) Distinctness [Eq. (12)] of the "large" dot heights from the "small" dot heights for spatially periodic heating (noise 1). d >0.5 represents usable distinctness.

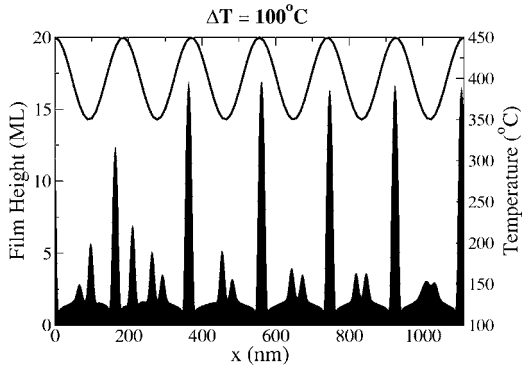

FIG. 10. Film height for periodic heating with $\Delta T=100\ ^{\circ}\mathrm{C}$ and $t=75$ s (noise 1). Distinctness $d=0.5$ [Eq. (12)]. Solid line indicates temperature profile.

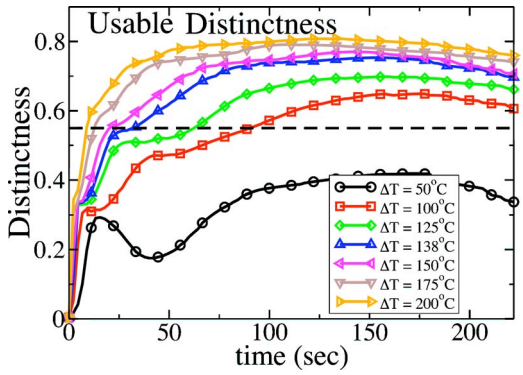

FIG. 12. (Color online) Distinctness of the "large" dot from the "small" dots [Eq. (13)] for Gaussian shaped heating (noise 1). $d>0.55$ indicates usable distinctness.

populations for the large dots to be spectroscopically different from the small dots. For each ΔT the distinctness is seen to improve with time (Fig. 9). Also, at any given instance, the rate of increase of distinctness is greater for higher ΔT values. The calculations for measuring distinctness have been done with noise 1 as the initial random noise fluctuation.

2. Spatial order

The spatial order is measured by calculating the standard deviation of the quantum dot spacings. A quantum dot spacing is measured as the distance between two quantum dot peaks (Figs. 2 and 3). Three different random initial conditions are taken into account and simulations done for three different ΔT values. The percentage standard deviations of the spacings for both spatially uniform and spatially periodic, averaged over the three different random noise realizations, are shown in Fig. 11. For most times and ΔT values, the average percentage standard deviations for periodic heating are lower than that of the uniform heating case, thus demonstrating that the periodic heating enhances spatial order.

B. Effectiveness of localized heating

The effectiveness of Gaussian shaped hot spot to produce a distinct single dot at a desired location is explored for its dependency on temperature and annealing times. As demonstrated in Sec. III, the simulations result in a large dot surrounded by a dot cluster, comprised of small dots. Also, there is a small misalignment between the desired location and the actual location of the large dot. Assuming that the small dot cluster would degrade device performance, the distinctness of the large dot from the other dots is an issue. In the following analysis the distinctness values are calculated as a function of temperature difference ΔT and annealing times t. The accuracy with which a distinct dot can be placed at a desired location is measured by calculating the misalignment between the achieved and desired locations. The misalignment values are also probed for its dependency on time t, temperature difference ΔT, and initial random noise fluctuation.

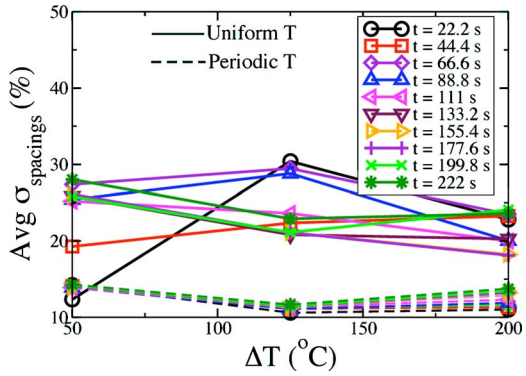

FIG. 11. (Color online) Percentage standard deviation of the quantum dot spacings averaged over noise patterns for spatially periodic heating.

1. Distinctness

Distinctness of the large dot from the small dots is defined in a way similar to the spatially periodic heating case [Eq. (12)];

$$d=\frac{h_{\mathrm{large}}-(\mu_{\mathrm{small}}+\sigma_{\mathrm{small}})}{h_{\mathrm{large}}}, \tag{13}$$

where h_{large}, μ_{small}, and σ_{small} refer to the height of the large dot, mean height of the small dots, and standard deviation of the heights of the small dots, respectively. In Fig. 4, h_{large} and $\mu_{\mathrm{small}}\pm\sigma_{\mathrm{small}}$ have been shown for $\Delta T=200\ ^{\circ}\mathrm{C}$ at two different stages of time. Figure 12 shows the distinctness values for various ΔT values. An acceptable distinctness value of 0.55 is defined. One such case with acceptable distinctness value of 0.55 for $\Delta T=100\ ^{\circ}\mathrm{C}$ is shown in Fig. 13. Any value of distinctness greater than the acceptable distinctness indicates usable distinctness or sufficient separation between the size of the large dot and the small dot clusters. The Gaussian temperature profile with temperature difference $\Delta T=50\ ^{\circ}\mathrm{C}$ is not effective enough in producing a distinct large dot within the considered annealing times range. However, for most other ΔT values listed and for most annealing times in Fig. 12, enough separation exists between the desired distinct dot and the small dots.

2. Misalignment

Misalignment is measured as the distance between the temperature peak and peak of the large dot (Fig. 4). Figure

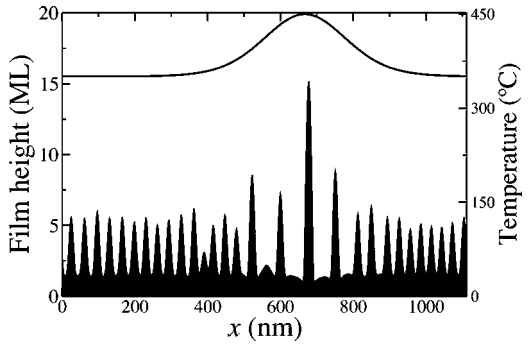

FIG. 13. Height profile for Gaussian shaped heating with a distinctness value of $d=0.55$ [Eq. (13)] at $t=89$ s and $\Delta T=100$ °C (noise 1). Solid line indicates temperature profile.

14 shows the misalignment values for ΔT values ranging from 50 to 200 °C and annealing times from 0 to 222 s. The discrete jumps in the misalignment values correspond to the mesh resolution. Hence, the misalignment values remain essentially constant in time and independent of T_{max} values, within the resolution of the simulations. However, the magnitude of misalignment varies with the random initial condition. In Fig. 15 the misalignment values are plotted for $\Delta T=138$ °C and annealing times ranging from $t=0-222$ s, corresponding to nine different random noise realizations. The rms value of the misalignment, corresponding to the nine different noise realizations, is calculated to be 12.5 nm, that is a misalignment of 5.6% of the full peak width of the Gaussian temperature profile.

V. CONCLUSIONS

Enhancement in the order of self-assembled epitaxial quantum dots and precision placement of a distinct quantum dot via thermal-field directed self-assembly have been demonstrated and quantitatively assessed for temperatures that might reasonably correspond to heating by a laser of wavelength about 180 nm. Simulations have been carried out for base temperatures of 350 °C and temperature differences ranging from 50 to 200 °C, also taking into account different random initial conditions. A spatially periodic form of heating and a Gaussian shaped hot spot have been used to study how spatially varying heating enhances both size and spatial orders, and can place a distinct quantum dot at a desired location, respectively.

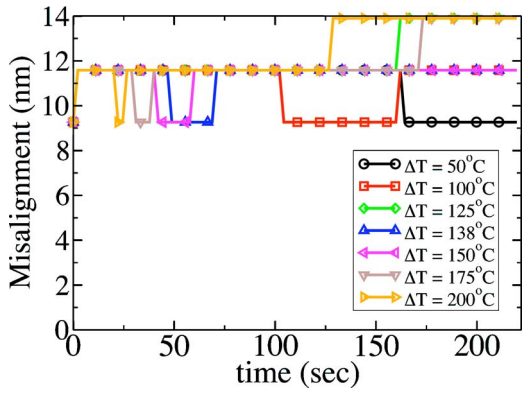

FIG. 14. (Color online) Misalignment of "large" dot (Fig. 4) vs time and temperature for Gaussian shaped heating (noise 1).

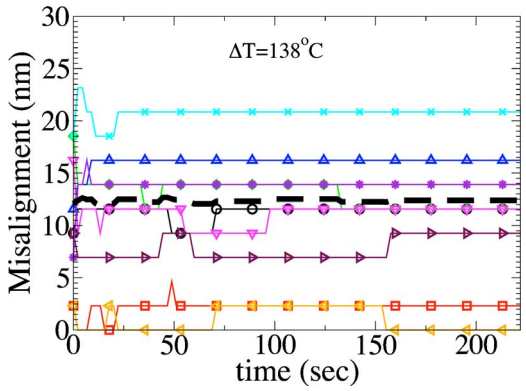

FIG. 15. (Color online) Misalignment of "large" dot (Fig. 4) resulting from Gaussian shaped heating at $\Delta T=138$ °C. The values for nine noise realizations are shown with different symbols. Bold dashed line is rms value.

Assuming a background temperature of 350 °C, it is possible to grow an array of quantum dots with enhanced order using a temperature peak as low as (350+25) °C. Sufficient distinctness of the "large" and "small" SAQD populations is achievable for a broad range of annealing times and peak temperature values. Localized heating is shown to result in a distinct quantum dot near the temperature peak for a broad range of peak temperatures. This single large dot is sufficiently distinct from the surrounding smaller dots for different temperatures and annealing times. It appears possible to place the large dot with 12.5 nm precision.

The specified thermal fields and their size ranges have been assumed to be achievable by using methods such as a laser interference pattern or heating with an electron beam. Thermal-field directed self-assembly of quantum dots represents an exciting possibility. For example, in addition to enhanced ordering, one might be able to write structures by sweeping a beam. These simulations only show the most basic potential, but clearly the possibilities warrant further investigation. This investigation should include experimental trials using surface heating by laser or other means and more sophisticated computational modeling similar to Ref. 14.

[1] M. Bayer, O. Stern, P. Hawrylak, S. Fafard, and A. Forchel, Nature (London) **405**, 923 (2000).
[2] T. Akiyama, H. Kuwatsuka, T. Simoyama, Y. Nakata, K. Mukai, M. Sugawara, O. Wada, and H. Ishikawa, IEEE Photonics Technol. Lett. **12**, 1301 (2000).
[3] E. A. Viktorov and P. Mandel, Appl. Phys. Lett. **88**, 201102 (2006).
[4] B. E. Kane, Nature (London) **393**, 133 (1998).
[5] J. M. Elzerman, R. Hanson, L. H. W. van Beveren, B. Witkamp, L. M. K. Vandersypen, and L. P. Kouwenhoven, Nature (London) **430**, 431 (2004).
[6] M. G. Tanner, D. G. Hasko, and D. A. Williams, Microelectron. Eng. **83**, 1818 (2006).
[7] L. H. Friedman and J. Xu, Appl. Phys. Lett. **88**, 093105 (2006).
[8] S. U. Hong, J. H. Lee, H.-S. Kwack, W.-S. Han, and D. K. Oh, J. Cryst. Growth **286**, 18 (2006).
[9] S. Y. Shiryaev, E. V. Pedersen, F. Jensen, J. W. Petersen, J. L. Hansen, and A. N. Larson, Thin Solid Films **294**, 311 (1997).
[10] S. Krishna, D. Zhu, J. Xu, and P. Bhattacharya, J. Appl. Phys. **86**, 6135 (1999).

[11]R. Hull *et al.*, Mater. Sci. Eng., B **101**, 1 (2003).
[12]O. Guise, J. J. T. Yates, J. Levy, J. Ahner, V. Vaithyanathan, and D. G. Schlom, Appl. Phys. Lett. **87**, 171902 (2005).
[13]COMSOL MULTIPHYSICS 3.2 (COMSOLAB, Stockholm, 2006), previously known as FEMLAB.
[14]Y. W. Zhang and A. F. Bower, Appl. Phys. Lett. **78**, 2706 (2001).
[15]A. A. Golovin, S. H. Davis, and P. W. Voorhees, Phys. Rev. E **68**, 056203 (2003).
[16]B. J. Spencer, P. W. Voorhees, and S. H. Davis, J. Appl. Phys. **73**, 4955 (1993).